



LAWRENCE
LIVERMORE
NATIONAL
LABORATORY

Measurement of cathodeluminescence efficiency of phosphors for micro-channel plate based x-ray framing cameras

N. Izumi, J. Emig, J. Moody, C. Middleton, J. Holder, S. Glenn, T. Pond, R. Shellman, M. Cardenas, P. J. Walsh, S. J. Chelli, D. K. Bradley, P. M. Bell

September 17, 2012

SPIE conference 8505 Target Diagnostics Physics and Engineering for Inertial Confinement Fusion
San Diego, CA, United States
August 12, 2012 through August 16, 2012

Disclaimer

This document was prepared as an account of work sponsored by an agency of the United States government. Neither the United States government nor Lawrence Livermore National Security, LLC, nor any of their employees makes any warranty, expressed or implied, or assumes any legal liability or responsibility for the accuracy, completeness, or usefulness of any information, apparatus, product, or process disclosed, or represents that its use would not infringe privately owned rights. Reference herein to any specific commercial product, process, or service by trade name, trademark, manufacturer, or otherwise does not necessarily constitute or imply its endorsement, recommendation, or favoring by the United States government or Lawrence Livermore National Security, LLC. The views and opinions of authors expressed herein do not necessarily state or reflect those of the United States government or Lawrence Livermore National Security, LLC, and shall not be used for advertising or product endorsement purposes.

Measurement of cathodeluminescence efficiency of phosphors for micro-channel plate based x-ray framing cameras

N. Izumi^{*a}, J. Emig^a, J. Moody^a, C. Middleton^a, J. Holder^a, S. Glenn^a, T. Pond^b, R. Shellman^b,
M. Cardenas^b, P. J. Walsh^c, S. J. Chelli^d, D. K. Bradley^a, P. M. Bell^a

^aLawrence Livermore National Laboratory, 7000 East Avenue, Livermore, CA, 94550;

^bNational Security Technologies, 161 S Vasco Road, Livermore, CA, 94551;

^cLos Alamos National Laboratory, 1350 Central, MS C330 Los Alamos, NM, 87545;

^dDeposition Research Laboratory, 530 Little Hills Industrial Blvd, St. Charles, MO, 63301

ABSTRACT

From a point of a signal-to-background ratio, phosphors are a key component of micro channel plate (MCP) based x-ray framing cameras. In an MCP based framing camera, x-ray signal is converted to electrons, gated, amplified, and converted back to optical signal on the phosphor. To operate x-ray framing cameras in a harsh neutron induced radiation background of the National Ignition Facility, cathodeluminescence efficiency of the phosphor is very important. To avoid MCP damage due to high voltage breakdown, we have been operating phosphors below 3kV (acceleration field < 6 kV/mm). The signal-to-background ratio the camera can be significantly improved by increasing the phosphor potential to 10kV. We measured conversion efficiencies of standard phosphors at electron energies of 0.5 ~10 keV and assessed achievable performance of them with using a numerical model.

Keywords: MCP, x-ray framing camera, neutron background, phosphor

INTRODUCTION

MCP based x-ray framing cameras are important diagnostics in inertial confinement fusion experiments at the National Ignition Facility [1]. On planned high neutron yield experiments, the expected neutron yield (14 MeV) can be 10^{17} or higher. In order to record x-ray emission images of the imploded core, x-ray framing cameras will have to be operated in that harsh neutron environment [2-9]. One of the simplest ways to increase signal level against the radiation background is use of higher phosphor potential.

For example, when the camera is located ~7m from the compressed plasma with no neutron shielding, the fluence of the 14MeV neutrons at the camera is about 1.6×10^{10} neutrons/cm². Those neutrons penetrate into the camera and excite the components of the camera. The radiation absorbed dose of the components can be estimated by using tabulated neutron KERAMA factors [10]. Most of the components consist of intermediate atomic number (Z = 12~29) elements have neutron KERMA factors of $1 \sim 2 \times 10^{-11}$ Gy·cm². Therefore the expected absorbed dose of the camera components is 160~300 mGy. In addition, gamma-rays produced by (n,n' γ) reactions around the camera will also deposit a similar amount of energy in the components [11]. This penetrating radiation causes ionization in the MCP, phosphor, fiber-optic face plate (FOFP), and recording device (typically a charge-coupled device (CCD) or a photographic film). It is known that radiation background on the MCP can be reduced by turning off the bias voltage before neutrons hit the MCP [6,12]. Radiation effects on the recording device can also be reduced by transferring the phosphor signal using image-relay optics and protecting the recording device with a massive radiation shielding enclosure [7-9]. However the phosphor and the FOFP are still exposed to the ionizing radiation with no significant shielding. For a phosphor thickness of 1mg/cm², the absorbed dose of 300mGy corresponds to a surface excitation of 0.3 μ J/cm². To achieve a good signal-to-background ratio, the electron excitation from the MCP has to be stronger than this radiation dose. The MCP output can be boosted by increasing electron multiplication gain in the MCP. However the maximum number of electrons we can extract from

the MCP is limited because the MCP shows nonlinear response for the output more than $1\text{nC}/\text{cm}^2$ [1,13]. Therefore it is necessary to increase the phosphor potential. If we set the phosphor potential to 3kV, the highest excitation density achievable in the MCP's dynamic range is up to $3\mu\text{J}/\text{cm}^2$. By raising the phosphor potential to 10kV, the excitation density can be increased to $9\mu\text{J}/\text{cm}^2$. In previous work, we measured absolute efficiency of phosphors up to 3kV using an MCP as a surface electron source [9]. It is now important to measure the absolute efficiency of the phosphors under 3~ 10 kV operation.

2. CONVERSION EFFICIENCY MEASUREMENT

Efficiencies of commonly used phosphors (Table 1) were tested using an electron-gun (Kimball EMB14 at NSTec, INC). Fig. 1 shows the experimental setup. All the phosphor samples are deposited on fiber optic face plates (INCOM B7D59-6, thickness: 7.87mm, numerical aperture 1.0, core percentage: 75%). Optical output from the phosphor was measured by a photometer (Photo Research, Pritchard PR-880). Focusing of the electron gun was adjusted to make a 25 mm +/- 5% diameter spot on the phosphor. The optical output was measured for phosphor potentials between 0.5 ~10kV. The electron current was adjusted (1 ~ 20nA) so that the excitation density to the phosphor is set to $\sim 2\mu\text{W}/\text{cm}^2$ regardless to the potential. The PR-880 unit has capability to be operated in a photometer mode (simulating spectral response of human eyes, measures luminance (cd/m^2)) and a radiometer mode (measures absolute radiance ($\text{watt}/\text{sr}/\text{m}^2$) on specific wavelength). Since this unit was calibrated only for the CIE photopic response, we operated the unit in the photometer mode.

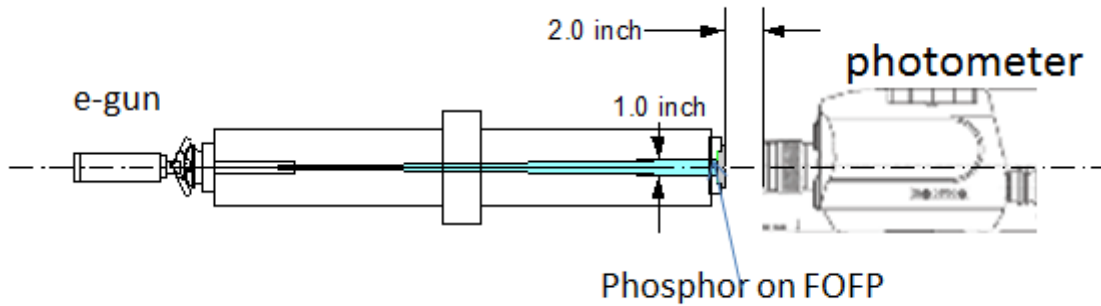


Fig. 1. Experimental setup of phosphor efficiency measurement.

Table 1. Phosphors tested

Type	Composition	Peak wavelength (nm)	Thickness	χ
P11	ZnS:Ag	450	1.2 mg/cm^2	0.5
P20	ZnCdS:Ag	540	1.2 mg/cm^2	0.33
P43	Gd ₂ O ₂ S:Tb	550	1.0 mg/cm^2	0.4
P46	Y ₃ Al ₅ O ₁₂ :Ce	530	1.0 mg/cm^2	0.35
P47	Y ₂ (SiO ₄)O :Ce	410	1.2 mg/cm^2	0.33

*the phosphors are deposited on the FOFP by Lexel Imaging Systems Inc. χ is experimentally determined coupling efficiency to the CCD with FOFP window which is directly contacted to the FOFP of the phosphor side.

With the photometer mode, the PR880 unit measures luminance L_v (cd/m^2) which is defined as,

$$L_v = 683 \int_{360\text{nm}}^{830\text{nm}} \frac{dR(\lambda)}{d\lambda} \cdot V(\lambda) d\lambda \quad (1)$$

where $dR(\lambda)/d\lambda$ is the absolute spectral radiance ($\text{watt}/\text{nm}/\text{sr}/\text{m}^2$) of the optical output through the FOFP, $V(\lambda)$ is a normalized 1931 CIE standard photopic response ($V(555\text{nm}) = 1$), the factor 683 is conversion factor from watts to lumen. In order to convert this luminance to radiance R ($\text{watt}/\text{sr}/\text{m}^2$), the sensitivity reduction of the photopic response on blue and red side was compensated,

$$R(\text{watt} / \text{sr} / \text{m}^2) = \frac{L_v}{683} \frac{\int_{360\text{nm}}^{830\text{nm}} T(\lambda) f(\lambda) d\lambda}{\int_{360\text{nm}}^{830\text{nm}} T(\lambda) f(\lambda) \cdot V(\lambda) d\lambda} \quad (2)$$

where, $f(\lambda)$ is the emission spectrum of each phosphor material, $T(\lambda)$ is the transmission of the FOFP. The signal intensity on a recording device coupled to the FOFP is given by irradiance E_e (watt/m^2) on the detector,

$$E_e(\text{watt} / \text{m}^2) = \chi \times \int_0^{2\pi} R(\theta) d\Omega \quad (3),$$

where χ is coupling efficiency of the FOFP output and the recording device determined by (1) fraction of effective area, (2) transmission of the input window, and (3) angular acceptance of the recording device. Because the photometer is sampling radiance of a solid angle on the FOFP's surface normal, we need to assume the angular distribution of the FOFP output. When the output is approximated by Lambertian distribution, an integration of the output over 2π steradian is,

$$E_e(\text{watt} / \text{m}^2) \approx \chi \times \pi \times R(0\text{deg}) \quad (4).$$

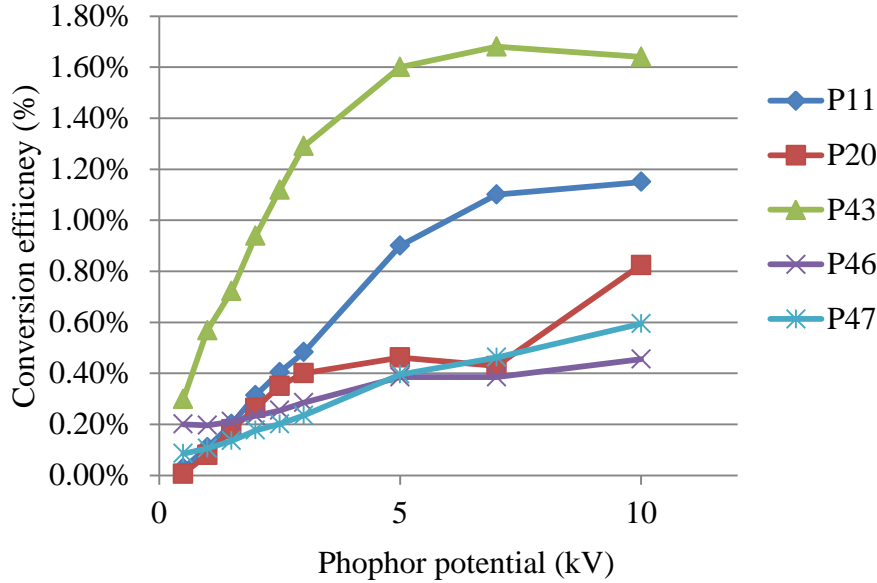


Fig. 2. Conversion efficiency vs phosphor potential. Data points below 3kV were measured with the MCP electron source and a calibrated CCD. Data points on 3~10kV were measured with the e-gun and the photometer.

The coupling efficiency χ for the CCD readout (0.3~0.5) is experimentally determined so that measurements with the photometer agree with the signal intensity on the CCD directly coupled to the FOFP [9]. The total conversion efficiency (including the deficiency of the FOFP) is calculated as

$$\eta = \frac{E_e \times S}{I \times V}, \quad (5)$$

where I is the electron beam current, V is the phosphor potential, and S is the beam spot area.

Fig. 2 shows the experimental result. Data points from 0.5-3kV are result of the MCP electron source with the CCD readout, 3-5 kV region are the e-gun and the photometer measurement. The conversion efficiency increased up to 5keV and showed a plateau over 7keV. The P43 sample showed the highest conversion among those samples.

3. NUMERICAL MODEL OF THE PHOSPHR

In order to optimize the phosphor thickness for 10kV operation, we performed a simple one-dimensional modeling of the electron transport in the phosphor.

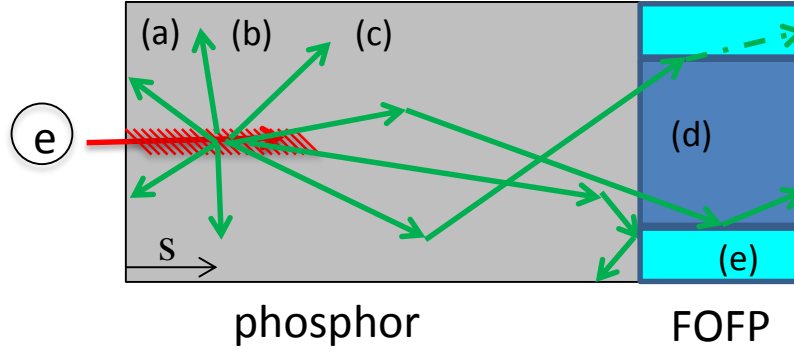


Fig. 3. Schematic of the electron/photon transport; (a) chemically degraded insensitive layer, (b) scintillating layer, (c) phosphor deeper than electron range, (d) core-glass of FOFP, (e) clad-glass of FOFP.

Figure 3 shows schematic of the electron and the photon transport in a phosphor. The 1st layer of the phosphor is a chemically degraded “dead layer”. This region absorbs electron energy but does not cause scintillation. Electrons penetrating through this dead layer cause scintillation in the 2nd layer. The 3rd layer is phosphor deeper than the range of the electrons. This layer does not making scintillations but does scatter photons from upstream. Some fraction of the photons is reflected back on the phosphor-glass boundary. Because the estimated reflective index of the phosphor is close to that of the core-glass ($n \sim 1.8$), a significant fraction of the photons reaching the boundary go into the core-glass. However because the numerical aperture of the FOFP is ~ 1.0 , rays entering with an incident angle more than ~ 34 degrees escape the core and are absorbed by the extra-mural absorber of the FOFP. The total conversion efficiency of the phosphor is thus approximated by,

$$CE = \eta_{phos} \eta_{trap} M \int_0^{\rho L} \left| \frac{dE}{ds} \right| \kappa(s) \zeta(s) ds \quad (6),$$

where η_{phos} is the intrinsic efficiency of the phosphor, η_{trap} is the light trapping efficiency of the FOFP, M is the reflectance factor which represents multiplication of the flux accounting for the rays scattered back to the FOFP, dE/dx is the estimated energy deposition of the electrons, ρL is the total thickness of the phosphor, $\kappa(s)$ and $\zeta(s)$ are depth dependent chemical degradation and light collection efficiency respectively. The trapping efficiency, η_{trap} is calculated as,

$$\eta_{trap} \approx F \frac{1 - \sqrt{1 - \left(N / \langle n_{phos} \rangle \right)^2}}{2}, \quad (7)$$

where F is the areal fraction of the core glass (75%), N is the numerical aperture of the FOFP (1.0), and $\langle n_{phos} \rangle$ is the averaged refractive index of the phosphor. Assuming $\langle n_{phos} \rangle = 1.8$, the estimated light trapping efficiency of the FOFP is ~6.3%.

For ease of calculation, the chemical degradation factor is modeled as,

$$\kappa(s) = 1 - \exp\left(-\frac{s}{\lambda_{chem}}\right) \quad (8)$$

where λ_{chem} is specific depth of the dead layer. Rigorously, the depth dependent coupling efficiency $\zeta(s)$ has to be calculated by solving complex photon transport inside the phosphor. The photons produced in the shallow region have less coupling to the FOFP because they have more chance to be scattered back in the downstream. In contrast, the coupling efficiency near the FOFP surface is enhanced because photons going away from the FOFP have more chance to be reflected back to the FOFP. Detailed transport of the photons in the scattering medium is described in [reference 12](#). However, since the thicknesses of our samples are less than the typical diffusion length of the phosphor (3~10 mg/cm² for 2-3 μ m gain size) [12], the scattering effect was ignored. Therefore $\zeta(s)$ and M are set to unity.

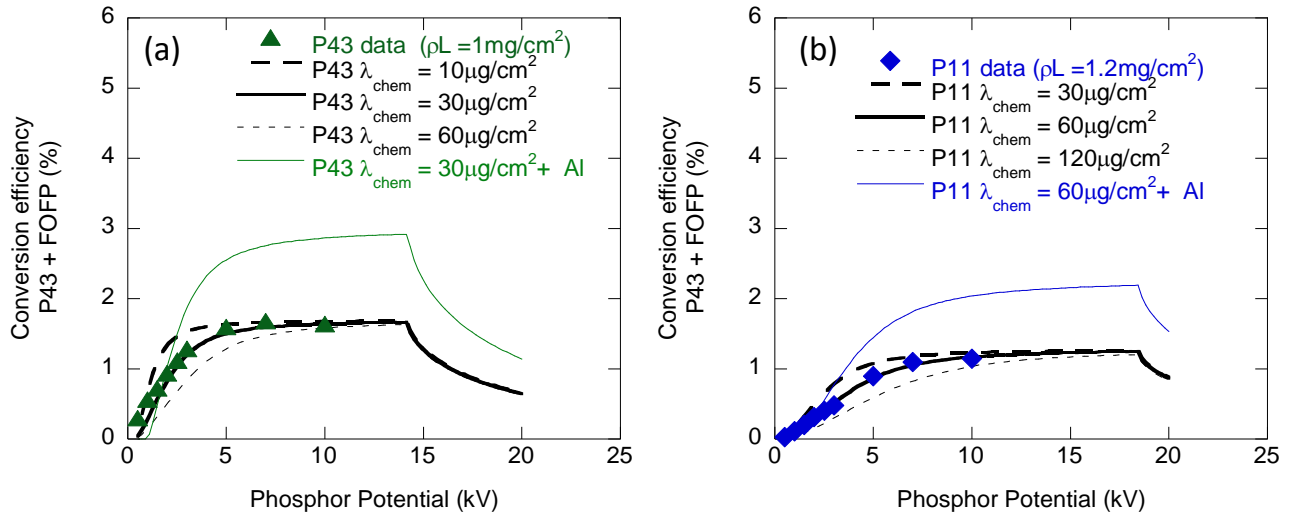


Fig. 3. Comparison of the experimental data and the numerical model. The experimental data points are plotted with efficiency calculated by Eq.(6).

Fig. 3 is a comparison of the experiment and the numerical model. Two parameters (η_{phos} and λ_{chem}) are adjusted so that the numerical model fits the experimental data. The response curve of the P43 sample was explained with $\eta_{phos} = 25\%$, $\lambda_{chem} = 30\mu\text{g}/\text{cm}^2$ ($\eta_{phos} = 19\%$, $\lambda_{chem} = 60\mu\text{g}/\text{cm}^2$ for P11). The sudden drop shown by the model on high energy side (~14 kV on P43 and ~18.5kV on P11) is due to electrons penetrating through the phosphor. The experiment up to 10kV did not show this sensitivity drop. Actual phosphors do not show this prominent drop because the phosphor thickness is not uniform and electrons are deflected inside the phosphor. Fig. 3 also shows the estimated phosphor output with a reflector coating (aluminum, 200 angstrom thick) on the phosphor. Due to electron energy loss in the reflector,

conversion efficiency below 3kV was significantly reduced. However due to light reflection on the reflector, expected output is increased by 70% at 10kV operation ($M \sim 1.7$).

4. SUMMARY

We measured conversion efficiencies of commonly used phosphors deposited on FOFP's. The best conversion efficiency is obtained when the phosphor thickness matches the stopping range of the electrons. When we operate the phosphors at a 10kV potential, a $\sim 1\text{mg/cm}^2$ phosphor provides maximum output. For operation below 5 kV, the use of an aluminum reflector coating is not beneficial. However over 5kV operation, reflection from the aluminum layer significantly increases the light collection efficiency. Compared to a conventional 3kV potential with no aluminum coating, the 10 kV operation with a 200 angstrom aluminum reflector can enhance the phosphor output by a factor 8x. This significantly improves the expected signal-to-background of x-ray framing cameras in a high radiation environment.

ACKNOWLEDGMENT

Lawrence Livermore National Laboratory is operated by Lawrence Livermore National Security, LLC, for the U.S. Department of Energy, National Nuclear Security Administration under Contract No. DE-AC52-07NA27344.

REFERENCES

- [1] J. D. Kilkenny, *Laser Par. Beams* **9**, 49 (1991).
- [2] R. A. Lerche, *Rev. Sci. Instrum.* **68**, 628(1997).
- [3] P. A. Jaanimagi, R. Boni, and R. L. Keck, *Rev. Sci. Instrum.* **72**, 801 (2001).
- [4] J. L. Bourgade, V. Allouche, J. Baggio, et al., *Rev. Sci. Instrum.* **75**, 4204 (2004).
- [5] C. Hagmann, N. Izumi, P. Bell, et al., *Rev. Sci. Instrum.* **81**, 10E514 (2010).
- [6] N. Izumi, C. Hagmann, G. Stone, et al., *Rev. Sci. Instrum.* **81**, 10E515 (2010).
- [7] J. L. Bourgade, R. Marmoret, S. Darbon et al, *RSI* **79**, 10F301 (2008)
- [8] P. M. Bell, D. K. Bradley, J. D. Kilkenny, et al., *Rev. Sci. Instrum.* **81**, 10E540 (2010).
- [9] N. Izumi, J. Emig, J. Moody, et al., *Proc. SPIE* **8142** 81420I-1 (2011).
- [10] R. J. Howerton, *Calculated Neutron KERMA Factors Based on the LLNL ENDL Data File*, UCRL-50400, Vol. 27 (January 1986)
- [11] C. Hagmann, private communication.
- [12] N. Izumi, G. Stone, C. Hagmann, et al., *Inst. Phys. Conf. Ser.* 244, 032048 (2010)
- [13] O. L. Landen, P.M. Bell, J. A. Oertel, et al., *Proc. SPIE* **2002**. 2 (1993).
- [14] G. E. Giakoumakis, C. D. Nomicos, and P. C. Euthymiou, *Can. J. Phys.* **59**, 88 (1981)